Applied Catalysis B: Environmental 113–114 (2012) 237–249

Contents lists available at SciVerse ScienceDirect

Applied Catalysis B: Environmental

journal homepage: www.elsevier.com/locate/apcatb

CO_2 hydrogenation at low temperature over Rh/γ-Al_2O_3 catalysts: Effect of the metal particle size on catalytic performances and reaction mechanism

Alejandro Karelovic*, Patricio Ruiz

Institute of Condensed Matter and Nanosciences (IMCN), Division Molecules, Solids and Reactivity (MOST), Université Catholique de Louvain, Croix du Sud, 2/17, 1348 Louvain-la-Neuve, Belgium

ARTICLE INFO

Article history:
Received 6 August 2011
Received in revised form
23 November 2011
Accepted 24 November 2011
Available online 2 December 2011

Keywords:
CO_2
Methanation
Rhodium
γ-Al_2O_3
Operando-DRIFTS
Transient MS
Particle size

ABSTRACT

Low temperature CO_2 methanation was studied on Rh/γ-Al_2O_3 catalysts. Catalysts were prepared with varying amounts of Rh to obtain different mean particle sizes, ranging between 3.6 and 15.4 nm. In the conditions studied, selectivity to methane was 100%. The intrinsic activity of Rh/γ-Al_2O_3 catalysts in CO_2 hydrogenation to methane was found to do not depend on particle size at temperatures between 185 and 200 °C, whereas at lower temperatures larger particles favored higher activity. Apparent activation energies were found to be in the range 14.5–22.7 kcal/mol. Lower activation energies were obtained for catalysts with larger particles. *Operando*-DRIFTS (Diffuse Reflectance Infrared Fourier Transform Spectroscopy) experiments showed that CO_2 is readily dissociated on these catalysts at 50 °C giving rise to different Rh carbonyl and formates species. Rh–CO species are proposed to be associated with H forming Rh carbonyl hydrides. According to transient experiments performed in different gas atmospheres, it is proposed that adsorbed CO is an important intermediate and that formates are spectators in the reaction path. Activation energy for CO dissociation is found to be similar to that of the overall reaction which suggests the importance of CO bond dissociation in the reaction path.

1. Introduction

It has been recognized that CO_2 is one of the main components of greenhouse gases and its concentration in the atmosphere has been continuously increasing due to the consumption of fossil fuels. The growing interest on greenhouse gas mitigation implies that CO_2 will be increasingly considered as a valuable feedstock for chemical industry instead as a waste [1,2]. There are different ways of adding value to CO_2, one of them is the hydrogenation to form methane (Eq. (1)).

$$CO_2 + 4H_2 \leftrightarrow CH_4 + 2H_2O \quad \Delta H^0 = -165\,kJ/mol \tag{1}$$

Provided that hydrogen is generated from renewable energy sources, the methane produced by this reaction can be sent to chemical industry or be utilized as an energy vector, which is an important advantage considering that the infrastructure for methane storage and transport is already present.

The major part of the studies concerning the methanation of CO_2, have been focused on the reaction performed at high temperatures (>200 °C) [3–6]. An important challenge in CO_2 reduction is the necessity of performing the reaction at low temperature in order to improve the flexibility of the operation, especially when CO_2 and/or H_2 sources are intermittent, and to ameliorate the energetic efficiency of the process. Nevertheless, the knowledge of the influence of the experimental parameters at low temperatures (<200 °C) process is very limited in the literature.

CO_2 methanation has been studied by several authors, using different noble metals such as Ru [7–11], Pd [3,12] and Rh [13–15] over a variety of supports. Among them Rh has been shown to be one of the most active metals.

It has been recently shown that the hydrogenation of CO_2 to form methane can be performed at room temperature over a Rh/γ-Al_2O_3 catalyst [16]. Other aspects of the reaction, specially the effect of adding CO and O_2 to the CO_2/H_2 feed have been studied recently [17]. When oxygen is added in low amount in the reactant gas feed, a positive effect in methanation is observed. For some CO_2/O_2 ratios, it was possible to obtain a higher conversion of CO_2 compared to those observed in the absence of oxygen. However, when the amount of oxygen is too high, oxygen has a negative effect. The same effects of oxygen have been observed in the case of the hydrogenation of CO [17]. The negative effect when the concentration of O_2 is high was explained by the over-oxidation of Rh. The reaction CO_2 methanation seems to be inhibited by CO. In presence of both CO_2 and CO, methane is produced exclusively from the methanation of CO.

The effect of metal particle size has not been studied in detail for CO_2 methanation on Rh catalysts. Results for other catalytic

* Corresponding author. Tel.: +32 10473651.
E-mail addresses: alejandro.karelovic@student.uclouvain.be, akarelov@gmail.com (A. Karelovic).

0926-3373/$ – see front matter © 2011 Elsevier B.V. All rights reserved.
doi:10.1016/j.apcatb.2011.11.043

systems seem to be contradictory. It has been shown that in the case of Ru/TiO_2 catalysts, highly dispersed metal forming small particles is more active than large metal ensembles [18]. For combined CO and CO_2 methanation, the same tendency has been reported over a Rh/Al_2O_3 catalyst [19]. On the contrary, other studies have shown that larger metal particles are more beneficial [20–22].

Concerning the mechanism of the reaction, different pathways have been proposed, which suggests that different catalytic formulations and operation conditions influence the mechanism of the reaction. It has been proposed that CO_2 dissociates to adsorbed CO and that the further dissociation of H_2CO produced by the stepwise hydrogenation of adsorbed CO is the rate-limiting step over a Rh/SiO_2 catalyst [23]. Recently, it has been suggested that CO_2 is dissociated in the surface of the catalyst to give adsorbed CO and adsorbed O over Ru/zeolite and Ru/Al_2O_3 catalysts [24]. It has been also proposed that adsorbed CO is produced by reverse water gas shift reaction through the formation and decomposition of formates species [7,10]. Moreover, it has been suggested that carbonates are likely intermediates of the reaction in the case of $Pd\text{-}Mg/SiO_2$ catalyst assuming that a bifunctional mechanism takes place over this type of catalysts [25].

In this work we present results concerning CO_2 methanation over $Rh/\gamma\text{-}Al_2O_3$ at low temperature (100–200 °C) and at atmospheric pressure. We discuss the influence of Rh particle size in the intrinsic catalytic activity. The apparent activation energy values obtained for different particle sizes are also discussed. The chemical state, dispersion and distribution of Rh on $\gamma\text{-}Al_2O_3$ support are studied by XPS analyses. Finally, the evolution of different surface species formed during the reaction is studied by *operando*-DRIFTS (Diffuse Reflectance Infrared Fourier Transform Spectroscopy) experiments and their implication in the mechanism of CO_2 methanation is discussed.

2. Experimental

2.1. Catalyst preparation

The catalysts were prepared by the wet impregnation method. $RhCl_3 \times xH_2O$ (Alfa Aesar, CAS 20765-98-4) was used as metallic precursor and the support was $\gamma\text{-}Al_2O_3$ (Alfa Aesar, CAS 1344-28-1, 99.97%). 5 g of support were suspended in 250 ml of distilled water. Appropriate amounts of Rh precursor were added to obtain catalysts with varying metal content (1, 1.5, 2, 3 and 5 wt.%). After stirring for 4 h and evaporating the solvent under reduced pressure in a rotavapor at 40 °C, the samples were dried at 110 °C overnight and then calcined in a static-air oven at 450 °C for 4 h (heating ramp 10 °C/min). Catalysts were afterwards grinded and sieved to obtain the appropriate grain size to be used in catalytic tests.

2.2. Characterization techniques

Surface area and pore volume of the support and catalysts were measured by N_2 adsorption and desorption isotherms at −196 °C using a Micromeritics Tristar 3000 instrument. Samples were degassed at 0.15 mbar and 150 °C overnight prior analysis. BET isotherm and BJH model were used to obtain specific surface area and pore volume, respectively.

X ray diffraction was performed on a Siemens D5000 diffractometer using Kα radiation of Cu. The 2θ range was scanned between 10 and 90° by steps of 0.02° with an acquisition time of 2 s at each step. Identification of the phases was carried out using the ICDD-JCPDS database.

H_2 chemisorption at 35 °C was used to measure the Rh exposed surface area. Experiments were performed with an ASAP 2010 C apparatus from Micromeritics. 0.15 g of catalyst were loaded into a Pyrex tube, and subsequently heated in He (20 ml/min) at 120 °C for 1 h. After evacuation, the sample was reduced at 350 °C during 1 h in pure H_2 (30 ml/min) followed by purging with He at the same temperature for 1 h and cooling in He to adsorption temperature. Two isotherms were measured in the range 0.07–90 kPa, the first corresponding to total adsorption, and the second to physisorbed H_2. The subtraction of the two isotherms gave the total amount of chemisorbed hydrogen. The amount of surface Rh atoms was calculated assuming that the chemisorption stoichiometry is H:Rh = 1 [26]. Dispersion is defined as surface Rh atoms divided by total Rh atoms in the catalyst. The mean particle size of Rh was calculated supposing they are hemispherical in shape, by the following equation:

$$d_p = \frac{6M}{D\rho\sigma N_0} \tag{2}$$

where M is the molecular weight of Rh (102.91 g/mol), D is the Rh fractional dispersion obtained as explained above, ρ is the Rh metal density (12.4 g/cm^3), σ is the area occupied by a surface Rh atom (7.58 Å^2/atom) and N_0 the Avogadro constant.

XPS analyses were performed with a SSI-X-probe (SSX-100/206) photoelectron spectrometer equipped with a monochromatic microfocused Al Kα X-ray source (1486.6 eV) from Surface Science Instruments. The sample powders were pressed into small stainless steel troughs mounted on a multi-specimen holder. The samples were outgased overnight under vacuum (10^{-5} Pa) and then introduced into the analysis chamber where the pressure was around 10^{-7} Pa. An electron flood gun set at 8 eV and a Ni grid placed at 3 mm above the sample were used to standardize charging effects. Pass energy of the analyser was 150 eV and the spot size was approximately 1.4 mm^2. The atomic concentration ratios were calculated by normalizing surface area ratios with sensitivity factors based on Scofield cross-sections. In addition, all binding energies were calculated taking as reference the C—(C, H) component of the C 1s adventitious carbon peak fixed at 284.8 eV. Peak decomposition was performed using the CasaXPS program (Casa Software Ltd., UK) with a Gaussian/Lorentzian (85/15) product function and a Shirley non-linear sigmoid-type baseline. The following peaks were used for the quantitative analysis: O 1s, C 1s, Al 2p, and Rh 3d.

The theoretical XPS intensity ratio Rh 3d/Al 2p (supposing monolayer coverage of Rh) was calculated according to the model proposed by Kerkhof and Moulijn [27] corresponding to the following equation:

$$\left(\frac{I_{Rh}}{I_{Al}}\right)_{mono} = \left(\frac{Rh}{Al}\right)_b \frac{D(\in_{Rh})}{D(\in_{Al})} \frac{\sigma_{Rh}}{\sigma_{Al}} \left(\frac{1-x}{\rho_{\gamma-Al_2O_3} \cdot S_{BET}}\right) \cdot \frac{1}{\lambda_{Al-Al}} \cdot \frac{(1+e^{-t/\lambda_{Rh-Al}})}{(1-e^{-t/\lambda_{Rh-Al}})}. \tag{3}$$

where $(Rh/Al)_b$ is the bulk atomic ratio calculated from the theoretical loadings of Rh. D factors are the spectrometer detection efficiencies, which are dependent on the kinetic energy of the electrons (ε). In this case, we approximate the D factors as $1/\varepsilon$ [27]. σ_{Rh} and σ_{Al} are the respective photoelectron cross sections, which were obtained from the tables of Scofield [28]. λ_{Al-Al} and λ_{Rh-Al} are the photoelectron escape depths for Al 2p electrons and Rh 3d electrons traversing $\gamma\text{-}Al_2O_3$ matrix, respectively. These values were obtained with the QUASES-IMFP-TPP2M software [29] which is based on the model proposed by Tanuma et al. [30]. $\rho_{\gamma-Al_2O_3}$ is the support density (4 g/cm^3) and S_{BET} is the BET surface area of $\gamma\text{-}Al_2O_3$.The sheet thickness of the support is defined as:

$$t = \frac{2\rho_{\gamma-Al_2O_3}}{S_{BET}}. \tag{4}$$

2.3. Operando-DRIFTS

In situ DRIFTS spectra were collected on a Bruker Equinox 55 infrared spectrometer equipped with an air-cooled MIR source with KBr optics and a MCT detector. Spectra were obtained by collecting 200 scans with a resolution of 4 cm^{-1} and are presented in absorbance mode without any manipulation. Samples were placed without packing or dilution inside a cell with controlled temperature and environment reflectance (Spectra-Tech 0030-102) equipped with ZnSe windows. The gases at the outlet of the cell were analyzed by a quadrupole mass spectrometer (Balzers QMS 200) by following the evolution of the m/z = 2 (H_2), 15 (CH_4), 18 (H_2O), 28 (CO) and 44 (CO_2).

The catalysts used in these experiments were previously reduced under hydrogen flow (30 ml/min) in a fixed bed reactor at 350 °C for 1 h and then grounded finely, before infrared experiments. Once the catalyst was placed in the cell, it was flushed in He (20 ml/min) for 10 min and then reduced again in a flow (20 ml/min) of a mixture of H_2 (10 vol.%) with He (90 vol.%), during 1 h at 300 °C. After that, the cell was cooled to 50 °C in the same gas mixture. Reaction was carried out introducing to the cell 20 ml/min of a mixture of CO_2 (2 ml/min), H_2 (8 ml/min) diluted in He (10 ml/min). The sample was kept at 50 °C for 20 min which was sufficient to ensure constant spectra. The system was then stepwise heated at 100 °C, 150 °C and 200 °C maintaining the sample 20 min at each temperature. Then, CO_2 was stopped and the sample was kept in H_2 (8 ml/min) diluted in He (10 ml/min) or pure He (18 ml/min) during 60 min at 150 °C or 200 °C. Spectra were recorded in all the above-mentioned steps.

2.4. Catalytic activity measurements

Catalytic tests were carried out using a quartz reactor (U-shaped) with 0.4 cm internal diameter. A section in the center of the tube is expanded with a diameter of 1 cm, in which the catalyst (200 mg, 200–315 μm particle size) was placed and supported by a quartz frit. A thermocouple was in contact with the central part of the catalyst bed and was used to measure and control the temperature. Heat and mass transfer effects were ruled out using the criteria recommended by Vannice [31]. Thus, one can safely assume that the reaction took place in fully kinetic regime.

The reaction was carried out at atmospheric pressure, by reducing the catalyst in a 30 ml/min flow of pure H_2 (Praxair 4.8) during 1 h (ramp 10 °C/min). Afterwards, the reactor was cooled to 50 °C and the reaction mixture (20 ml/min) was admitted (CO_2 (Praxair 4.8, 10 vol.%), H_2 (40 vol.%) diluted in He (Praxair 4.8)). Measurements were performed at various temperatures between 50 and 200 °C (with 1 h at each temperature to ensure steady state). Exit gases were analyzed by gas chromatography (CH_4 and CO_2 were detected using FID and TCD detectors, respectively). All transfer lines were maintained at 120 °C to avoid water condensation.

Reaction rates were determined always when CO_2 conversion was less than 10% to ensure differential reactor conditions. Reaction rates are expressed as the number of moles of CH_4 produced by mole of Rh by second or as turnover frequencies (TOF), namely, as the number of moles of CH_4 produced by moles of Rh on the surface by second. The number of moles of Rh on the surface was obtained from dispersion data.

3. Results

3.1. Characterization of materials

Textural properties and dispersion of the prepared Rh/γ-Al_2O_3 catalysts are presented in Table 1. All samples show isotherms characteristic of non-porous solids. Comparing with pure γ-Al_2O_3 that was calcined in the same conditions as the catalysts, the surface area was very similar to the support and among all the catalysts, varying slightly with Rh content. The pore volume increases after impregnation and calcination.

X ray diffraction results (not shown) confirm the presence of γ-Al_2O_3 (2θ = 45 and 65°) phase after calcination. No peaks coming from Rh related diffraction peaks were observed.

Supported Rh was found to have different dispersion depending on the amount of Rh loaded. The highest dispersion was 0.30 for the catalyst with 1 wt.% Rh content whereas when the Rh content surpasses 3 wt.% the dispersion stabilizes around 0.07. Particle sizes obtained from dispersion data are also shown in Table 1. It is observed that Rh particle size increases from 3.6 to 15 nm when the amount of Rh content increases from 1 wt.% to 5 wt.%.

3.2. Activity results

Table 2 shows the results concerning CO_2 hydrogenation for all catalysts prepared. Catalytic activity depends on the temperature. At 150 °C, the catalytic activity by mol of total Rh atoms does not vary appreciably with Rh loading. At 200 °C, the activity decreases with the Rh content and it is the higher for Rh(1%)/γ-Al_2O_3 catalyst which is nearly 6 times more active than Rh(5%)/γ-Al_2O_3 catalyst. Regarding TOF values at 200 °C, the activity seems to vary only slightly with loading, whereas at 150 °C intrinsic rates are found to increase with Rh loading.

The effect of Rh dispersion on activity is presented in Fig. 1a. The rate of methane production per total Rh content is plotted as a function of dispersion, for different temperatures. The activity increases significantly with dispersion at high temperature (165–200 °C), whereas when the temperature is lower (135–150 °C), the variations in activity are much less pronounced. In Fig. 1b it is shown the variation of turnover frequencies (the rate of methane formation per Rh atoms on the surface) with dispersion. At low temperature, the turnover frequencies tend to decrease when dispersion increases. At higher temperatures this tendency is attenuated and for instance at 185 and 200 °C, the slope is nearly zero. Apparent activation energies were obtained in the range 135–200 °C and are shown in Table 2. It is observed that the apparent activation energy decreases with decreasing Rh dispersion (or increasing Rh content).

3.3. XPS results

In Fig. 2 are shown the Rh 3d XP-spectra of Rh(1%)/γ-Al_2O_3 (a) and Rh(5%)/γ-Al_2O_3 (b) catalysts after calcination at 450 °C during 4 h (1), CO_2 hydrogenation (2) and reduction under pure H_2 at 350 °C for 1 h (3). The measured spectra were fitted by two doublets, one fixed at 307–307.3 eV assigned to Rh in a metallic form (Rh^0 species) [32–34], and another that can be related to different oxidized species. We could not further decompose this doublet to differentiate the various oxidation states present on the samples, because the calculation yielded more than one solution. Regarding the peak related to oxidized species, it has been reported that Rh $3d_{5/2}$ electrons from Rh^{3+} have binding energies between 308.1–308.4 eV [33,34]. Rh $3d_{5/2}$ peak positions in the order 309.3–309.9 eV have been assigned to Rh^{4+} species [33] or to non-stoichiometric Rh_2O_3 (Rh^{3+}) in which the outermost layers have O/Rh ratios higher than 1.5 [33]. In the case of Rh(1%)/γ-Al_2O_3 after calcination (Fig. 2a, trace 1) the Rh $3d_{5/2}$ doublet presents one peak at 309.8 eV characteristic of oxidized Rh (Rh^{4+} or non-stoichiometric Rh_2O_3). The other peak which accounts for 6% of the Rh, appears at 307.3 eV, thus indicating Rh metallic species. When the sample is reduced at 350 °C for 1 h in H_2 (Fig. 2a, trace 2), the Rh 3d spectrum shifts to lower binding energies. Besides the Rh^0 component which has grown to 26% of the total detected Rh, the

Table 1
N_2 adsorption and H_2 chemisorption results for Rh/γ-Al_2O_3 catalysts.

Samples	BET surface area (m^2/g)	Pore volume BJH (cm^3/g)	Metal dispersion (H/Rh)	Rh mean particle size (nm)
γ-Al_2O_3[a]	71	0.26	–	–
Rh (1%)/γ-Al_2O_3	68	0.37	0.30	3.6
Rh (1.5%)/γ-Al_2O_3	67	0.37	0.24	4.5
Rh (2%)/γ-Al_2O_3	71	0.38	0.18	6.1
Rh (3%)/γ-Al_2O_3	71	0.28	0.071	15.4
Rh (5%)/γ-Al_2O_3	65	0.33	0.072	15.1

[a] Pure γ-Al_2O_3 was calcined at the same conditions as the catalysts.

Table 2
Kinetic measurements for Rh/γ-Al_2O_3 catalysts in CO_2 hydrogenation at 150 °C and 200 °C.

Catalyst	150 °C		200 °C		Activation energy (kcal/mol)
	Rate × 10^2 (mol CH_4/mol Rh/s)	TOF × 10^2 (mol CH_4/mol Rh (surf)/s)	Rate × 10^2 (mol CH_4/mol Rh/s)	TOF × 10^2 (mol CH_4/mol Rh (surf)/s)	
Rh 1 wt.%/γ-Al_2O_3	0.028	0.092	0.516	1.720	22.7
Rh 1.5 wt.%/γ-Al_2O_3	0.028	0.115	0.298	1.241	19.1
Rh 2 wt.%/γ-Al_2O_3	0.041	0.228	0.273	1.515	15.8
Rh 3 wt.%/γ-Al_2O_3	0.024	0.333	0.133	1.878	14.6
Rh 5 wt.%/γ-Al_2O_3	0.015	0.203	0.086	1.193	14.5

Rh $3d_{5/2}$ doublet shows a peak at 308.8 eV, thus, decreasing 1 eV comparing with the spectrum taken after calcination. The Rh 3d spectrum taken after the reaction is shown in Fig. 2a trace 3. There are no significant changes comparing with the catalyst after reduction, the position of the peaks and the relative intensity did not change appreciably.

XPS results for Rh 3d electrons region for Rh(5%)/γ-Al_2O_3 are presented in Fig. 2b. The spectrum for calcined catalysts is similar to that for calcined Rh(1%)/γ-Al_2O_3, Nearly all the Rh species analyzed are in oxide form. When the catalyst is subjected to reaction or reduction in H_2, two kinds of Rh species are found, namely Rh^0 with peak center at 307.1 eV and oxidized species (Rh^{n+}) which peak appears at 308.9 eV. The proportion of reduced Rh species is between 60 and 70% compared to Rh (1%)/γ-Al_2O_3 which has a proportion of Rh reduced species around 30%.

The spectra for the other catalysts are not shown for the sake of brevity. Nevertheless, the results for all the catalysts are shown in Table 3.

Table 3 shown the XPS results obtained for calcined, reduced and after reaction catalysts. The XPS Rh/Al atomic ratios increase with the Rh content. Samples show a clear decrease in the XPS Rh/Al atomic ratios after reduction treatment, except in the case of Rh(1 wt.%)/Al_2O_3 which shows a XPS Rh/Al atomic ratio nearly unchanged after reduction. When samples were subjected to reaction, the XPS Rh/Al atomic ratio remains essentially unchanged (comparing with calcined samples), except for Rh(5 wt.%)/Al_2O_3 which presents a clear decrease in its XPS Rh/Al atomic ratio.

When comparing XPS Rh/Al atomic ratios with the bulk Rh/Al atomic ratios (Table 3), in all the catalysts, the XPS Rh/Al atomic ratio ratios are higher than the bulk ones by a factor between 2 and 3.

It is worth noting that XPS atomic concentrations and binding energies of C 1s (284.8 eV), Al 2p (74.4–74.5 eV) and O 1s (531.2–531.3 eV) did not show significant changes in the course of the different treatments applied and therefore they are not shown.

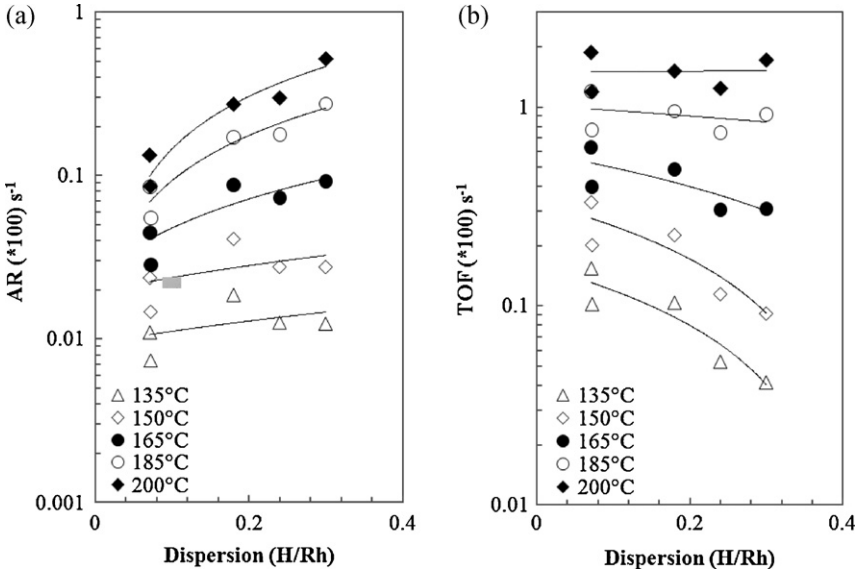

Fig. 1. Rate of CH_4 formation as a function of Rh fractional dispersion, measured at different temperatures. Data were collected after 1 h of reaction at each temperature. (a) Atomic rate of CH_4 formation (AR, mol CH_4/mol Rh/s). (b) Turnover frequencies (TOF, mol CH_4/mol Rh on surface/s).

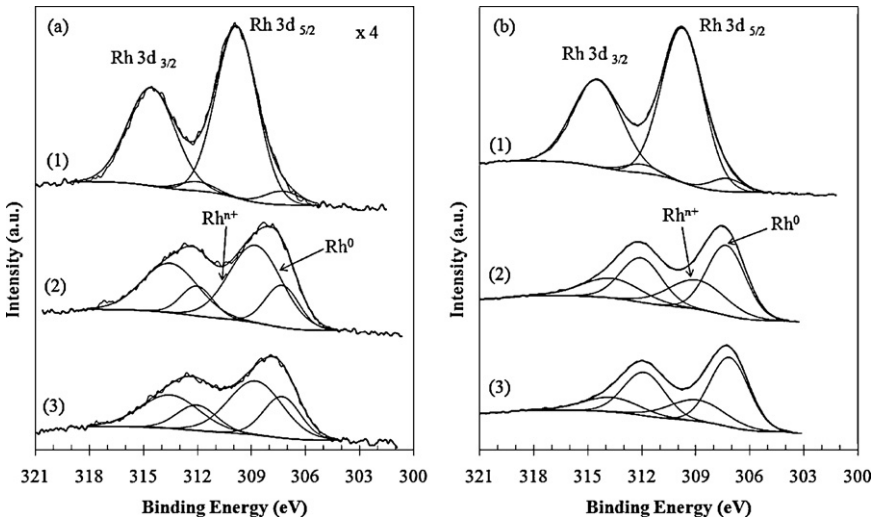

Fig. 2. XP-spectra of Rh 3d electrons for (a) Rh (1%)/γ-Al_2O_3 and (b) Rh (5%)/γ-Al_2O_3 subjected to different treatments, oxidation states are indicated in the figure. (1) Catalyst calcined at 450 °C for 4 h; (2) Catalyst after reduction at 350 °C during 1 h (H_2 30 ml/min); (3) Catalyst recovered after catalytic test.

In Fig. 3 it is shown the intensity ratio I_{Rh}/I_{Al} obtained by XPS and the intensity ratio I_{Rh}/I_{Al} calculated following the Kerkhof's model, assuming that the Rh was dispersed forming a monolayer on the surface of γ-Al_2O_3. It can be observed that for all the catalysts the XPS I_{Rh}/I_{Al} ratios obtained experimentally are higher than those obtained by the Kerkhof's model.

3.4. Operando-DRIFTS results

3.4.1. Steady state reaction conditions ($CO_2 + H_2$)

In Fig. 4 are shown DRIFT spectra obtained for Rh(1%)/γ-Al_2O_3, Rh(2%)/γ-Al_2O_3 and Rh(5%)/γ-Al_2O_3 catalysts and γ-Al_2O_3 in presence of a mixture of H_2 and CO_2 between 50 and 200 °C. All spectra were recorded after 20 min at each temperature. The samples have been previously reduced ex-situ in pure hydrogen at 350 °C and afterwards re-reduced inside the DRIFTS cell at 300 °C in 20 ml/min of H_2(10%)/He before reaction.

The range between 1200 and 2200 cm^{-1} was found to be the representative of the adsorbed species observed. The hydroxyl region (3000–3700 cm^{-1}) does not show significant changes, neither the region of lower wavenumbers which was highly perturbed by experimental noise. The CH_x vibrations reported to appear in the 2800–3000 cm^{-1} region [11] were not detected in our experiments.

The spectrum obtained for Rh(1%)/γ-Al_2O_3 at 50 °C (Fig. 4A, trace a) show the apparition of a strong band centered at 2036 cm^{-1} which can be assigned to CO species linearly bonded to Rh (Rh^0—CO) [13,23,35–37]. The tail observed at lower wavenumbers has been ascribed to carbonyls bonded to different types of metal surfaces [38,39].

There is also the formation of a strong band at 1630 cm^{-1} which can be assigned to water adsorbed on the support [40]. Bands assigned to asymmetric and symmetric bending O—C—O vibrations of adsorbed formate ions can be observed at 1587, 1370 and 1390 cm^{-1} [11,41]. A band appearing at 1460 cm^{-1} which is commonly associated to carbonates [11], is also observed.

When the temperature is raised to 100 °C, the band related to Rh carbonyls increases in intensity, as well as the bands attributed to formates and carbonates (trace b). At this temperature water is desorbed and the intensity of the 1640 cm^{-1} band decreases accordingly. Further heating continues to increase the intensity of the Rh-CO band and at the same time there is a change in its position to lower wavenumbers, reaching 2021 cm^{-1} at 200 °C. A broad band at 1805 cm^{-1} is also detected. This band is attributed to bridge-bonded CO on Rh (Rh^0_2-CO) [35,42–44]. The formate bands (1587, 1370 and 1390 cm^{-1}) increase in intensity when temperature is raised. The band assigned to carbonates (1460 cm^{-1})

Table 3
XPS results for all the prepared catalysts following calcination (C), reduction (R) and catalytic test (T).

Sample Rh/γ-Al_2O_3		Rh/Al XPS	Rh/Al bulk	Rh $3d_{5/2}$ oxidized			Rh $3d_{5/2}$ reduced		
				Position (eV)	FWHM (eV)	%	Position (eV)	FWHM (eV)	%
1 wt.%	C	0.0128		309.8	2.68	94	307.3	2.28	6
	R	0.0127	0.0050	308.8	3.44	74	307.3	2.20	26
	T	0.0124		308.8	3.53	66	307.3	2.40	34
1.5 wt.%	C	0.0173		309.7	2.69	95	307.3	2.15	5
	R	0.0155	0.0075	308.7	3.45	64	307.3	2.23	36
	T	0.0174		308.8	3.70	52	307.3	2.39	48
2 wt.%	C	0.0239		309.7	2.74	96	307.3	2.22	4
	R	0.0227	0.0101	308.8	3.39	61	307.3	2.13	39
	T	0.0222		308.7	3.30	68	307.3	2.01	32
3 wt.%	C	0.0369		309.7	2.66	94	307.3	2.23	6
	R	0.0309	0.0153	308.8	3.51	51	307.3	2.21	49
	T	0.0380		308.8	3.55	60	307.3	2.27	40
5 wt.%	C	0.0574		309.7	2.72	94	307.3	2.08	6
	R	0.0551	0.0261	308.9	3.73	38	307.3	2.51	62
	T	0.0470		308.9	3.66	31	307.1	2.53	69

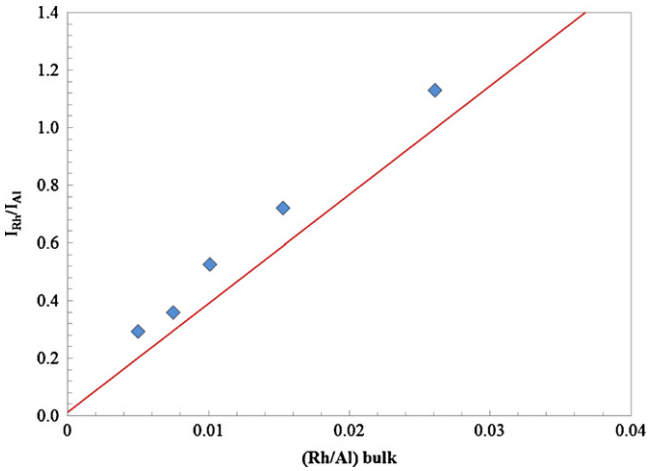

Fig. 3. Calculated and measured XPS intensity ratios for Rh/γ-Al_2O_3 catalysts as a function of Rh/Al bulk ratios. Diamonds indicate the measured I_{Rh}/I_{Al} intensity ratios and the line represent the theoretical I_{Rh}/I_{Al} XPS ratio calculated for a monolayer of Rh on γ-Al_2O_3.

does not change appreciably its intensity. Regarding the other catalysts with higher Rh loading, the spectral features are similar to Rh(1%)/γ-Al_2O_3, but some differences appear. In the case of Rh(2%)/γ-Al_2O_3 catalyst at 50 °C (Fig. 4B, trace a), the peak due to linear Rh-CO species appears at somewhat higher wavenumbers (2040 cm^{-1}). Another different feature is the formation of a very weak band at 1905 cm^{-1}, which can be related to the formation of $Rh_2(CO)_3$ species [23,44]. Upon further heating this weak band disappears and the Rh-CO band increases in intensity and shifts to lower wavenumbers reaching 2023 cm^{-1} at 200 °C (trace d). In the case of Rh(5%)/γ-Al_2O_3 (Fig. 4C), at 50 °C the band due to Rh-CO linearly adsorbed shows two peaks, the more intense at 2052 cm^{-1} and the weaker appearing at 2027 cm^{-1}. The peak that has been attributed to bridged $Rh_2(CO)_3$ dimer (1905 cm^{-1}) appears with more intensity than for the other catalysts. Further heating to 200 °C leads to the disappearance of this peak. The band attributed to linearly adsorbed CO continues to increase in intensity while it shifts to 2027 cm^{-1}. The broad band located at 1805 cm^{-1}, attributed to bridge-bonded CO on Rh increases its intensity to reach a maximum at 150 °C.

In Fig. 4D are shown the spectra obtained for pure γ-Al_2O_3. At 50 °C one can only detect an intense peak at 1630 cm^{-1}, that, as already said, is due to the presence of adsorbed water. This peak disappears with further heating. The peak due to carbonates (1460 cm^{-1}) is present in this sample, and increases slightly in intensity with temperature. There is another peak appearing at 1579 cm^{-1} which can be assigned to carbonates and as in the case of 1460 cm^{-1} peak, its intensity does not change appreciably with temperature. No peaks attributed to linear CO adsorbed species were observed over γ-Al_2O_3.

3.4.2. Hydrogenation of adsorbed species

Results concerning the transient behavior of surface species that were formed during reaction conditions ($H_2 + CO_2$) at 150 °C and 200 °C and were subsequently exposed to a flow of H_2 are presented in Figs. 5 and 6.

Fig. 5 shows the spectra obtained at 150 °C. In the case of Rh(1%)/γ-Al_2O_3 catalyst (Fig. 5A), it can be seen that in presence of H_2, the band related to CO adsorbed on Rh^0 (2036 cm^{-1}) decreases in intensity with time. The same behavior can be observed for the bands at 1593 and 1390–1370 cm^{-1}, which are due to surface formate species. In contrast, the weak band at 1460 cm^{-1} does not change appreciably in intensity with time. The behavior of the bands characteristic of surface formates observed for Rh(2%)/γ-Al_2O_3 and Rh(5%)/γ-Al_2O_3 catalysts (Fig. 5B and C, respectively), is similar to that found for Rh(1%)/γ-Al_2O_3. In the case of the band related to CO bonded linearly to Rh (2029 cm^{-1}), for Rh(2%)/γ-Al_2O_3, the band decreases in intensity with time and at the same time a small peak appearing at 1910 cm^{-1}, assigned to $Rh_2(CO)_3$ develops after 20 min in H_2. For Rh(5%)/γ-Al_2O_3, the decrease of linear Rh-CO band is more rapid and is accompanied by a shift from 2032 cm^{-1} to 2025 cm^{-1}. As for the Rh (2%)/γ-Al_2O_3 the band that have been assigned to $Rh_2(CO)_3$ starts to grow with time reaching a maximum at about 20–25 min. In this sample one can also observe that the broad band of bridged $Rh_2(CO)$ (1805 cm^{-1}) species decrease rapidly and has completely disappeared after 25 min on H_2 stream.

Table 4
Activation energies for CO dissociation obtained in transient DRIFTS experiments in H_2. Flow composed of H_2 (8 ml/min) + He (10 ml/min), activation energies calculated for temperatures between 150 and 200 °C.

Catalyst	E_a (kcal/mol)
Rh(1%)/γ-Al_2O_3	21
Rh(2%)/γ-Al_2O_3	23
Rh(5%)/γ-Al_2O_3	16

Fig. 6 shows the transient behavior of the same catalysts when exposed to H_2 at 200 °C following $H_2 + CO_2$ reaction at the same temperature. In this case, it can be clearly seen that the rate of disappearance of adsorbed species is higher. In the case of Rh(1%)/γ-Al_2O_3 catalyst (Fig. 6A), the band assigned to linear Rh-CO species decreases rapidly accompanied by a shift to lower wavenumbers from 2021 to 2005 cm^{-1} but it does not disappear completely after 40 min of exposure to H_2. The band corresponding to $Rh_2(CO)$ (1800 cm^{-1}) in bridged form disappears readily after 5 min on stream. Regarding the band arising from carbonate species (1460 cm^{-1}), its intensity does not vary with time, whereas the formate bands (1590 and 1370–1390 cm^{-1}) are found to decrease with time on stream. The other catalysts shown in Fig. 6 behave similarly, with the linearly adsorbed CO band decreasing rapidly, and after 15–20 min the bands stabilize with a very weak intensity. At the same time, there is a frequency shift toward lower values, between 2003 and 2005 cm^{-1}.

The intensity ratios of carbonyl (2000–2040 cm^{-1}) and formate (1595 cm^{-1}) bands were calculated taking as reference the peak area right before gas switching. Intensity ratios were plotted in function of time (Fig. 7). In the case of Rh-CO species, the calculations were done for linearly bonded CO whose signal is much more intense and well-defined comparing to bridged bonded CO bands.

It can be observed that the intensity of CO band decreases steadily in time, and that the rate of disappearance depends on Rh content, Rh(5%)/γ-Al_2O_3 being the one with the faster rate. Regarding formate bands (1593 cm^{-1}), Fig. 7B shows that these bands decrease erratically with time and at a much slower rate comparing with carbonyl bands. Even after 40 min of exposure to H_2, the bands still have more than 80% of their initial intensity.

Activation energies for the dissociation of adsorbed CO are shown in Table 4. These values were obtained taking into account the rates of Rh-CO peak disappearance at 150 °C and 200 °C. The activation energies lie between 16 and 23 kcal/mol, showing a good agreement with the results show in Table 2 for the activation energy of the whole CO_2 hydrogenation process.

The evolution of CH_4 during DRIFTS experiments is shown in Fig. 8. The formation of methane can be observed at 150 °C for all the catalysts studied. No other product was observed either by gas chromatography in fixed-bed reactor tests or by MS in DRIFTS.

Upon stopping CO_2 feed, the concentration of CH_4 starts to decrease. In the case of catalysts with low Rh content (1% and 1.5%) the signal of CH_4 decreases steeply when CO_2 is stopped, and

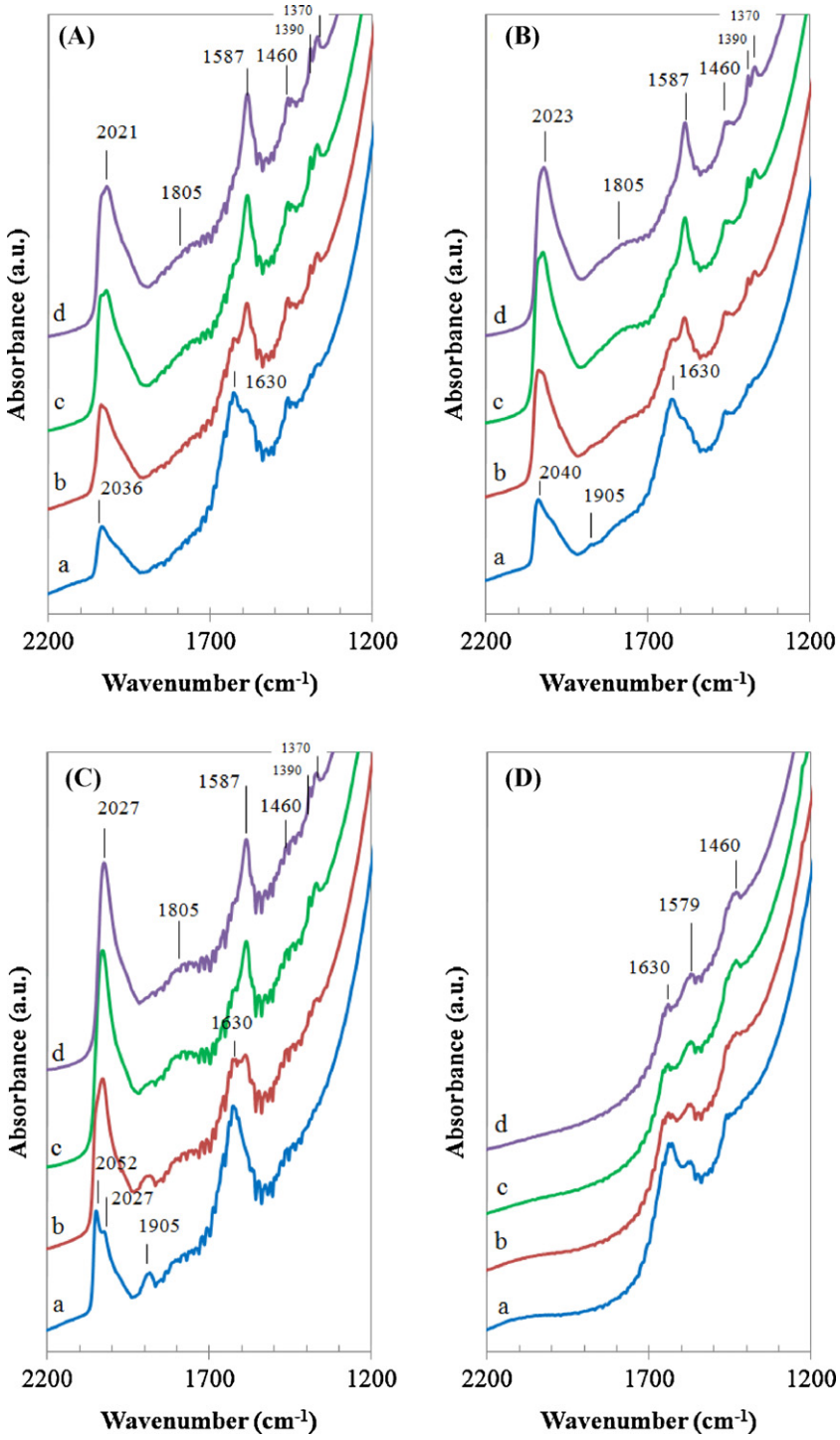

Fig. 4. DRIFT spectra for (A) Rh (1%)/γ-Al_2O_3, (B) Rh (2%)/γ-Al_2O_3, (C) Rh (5%)/γ-Al_2O_3 and (D) γ-Al_2O_3 under reaction conditions (CO_2 2 ml/min + H_2 8 ml/min + He 10 ml/min) at (a) 50 °C, (b) 100 °C, (c) 150 °C and (d) 200 °C. All spectra were recorded after 20 min stabilization at each temperature.

afterwards the production of CH_4 is essentially constant to further decrease after 25–30 min in H_2 flow. Catalysts with higher Rh content show a more smooth decrease of CH_4 concentration with time. Nevertheless, all the catalysts show methane production up to more or less 30 min in H_2 flow.

3.4.3. *Transient experiments with H_2 + He and pure He*

Fig. 9A shows the spectra obtained for Rh(5%)/γ-Al_2O_3 when $H_2 + CO_2$ flow is changed to pure He. It can be observed that the CO carbonyl band located at 2030 cm^{-1} starts to decrease in intensity and after 40 min it has a very weak intensity. The position of the band does not change, staying at 2030 cm^{-1} even when its intensity is very low after 60 min of exposure to He. The band located at 1810 cm^{-1} characteristic of CO adsorbed in a bridged form increases its intensity when He is admitted to the cell reaching a maximum at 10 min to disappear at 30 min. Formate and carbonate bands do not change appreciably during this experiment. In Fig. 9B it is shown for comparison the spectra obtained for Rh(5%)/γ-Al_2O_3 catalyst when the flow is changed to H_2 + He. In this case one important difference is that the rate of linear Rh-CO

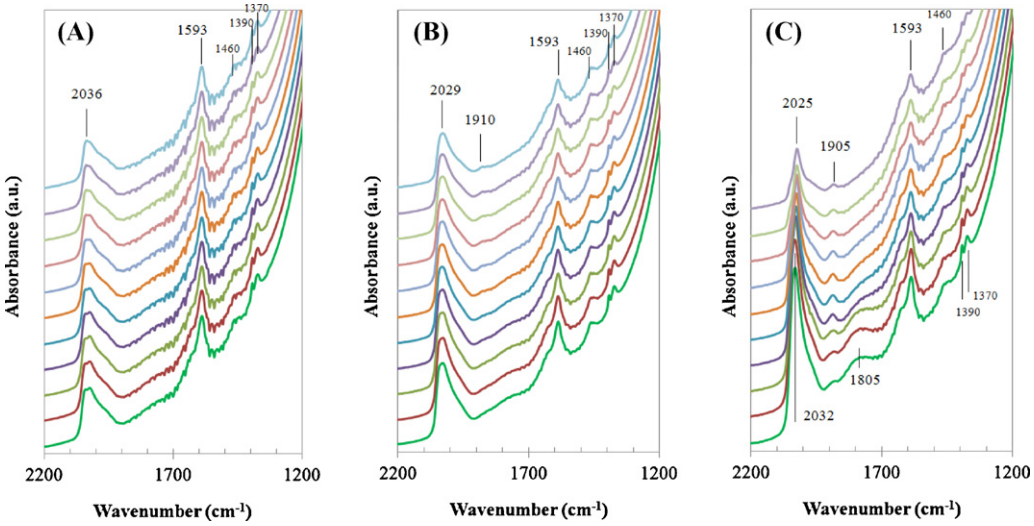

Fig. 5. DRIFT spectra for (A) Rh (1%)/γ-Al_2O_3, (B) Rh (2%)/γ-Al_2O_3, (C) Rh (5%)/γ-Al_2O_3 catalysts after the flow composed of H_2 (8 ml/min) + CO_2 (2 ml/min) + He (10 ml/min) is switched to H_2 (8 ml/min) + He (10 ml/min) at 150 °C. From bottom to top: before gas change, after 1, 5, 10, 15, 20, 25, 30, 35, 40 and 50 min.

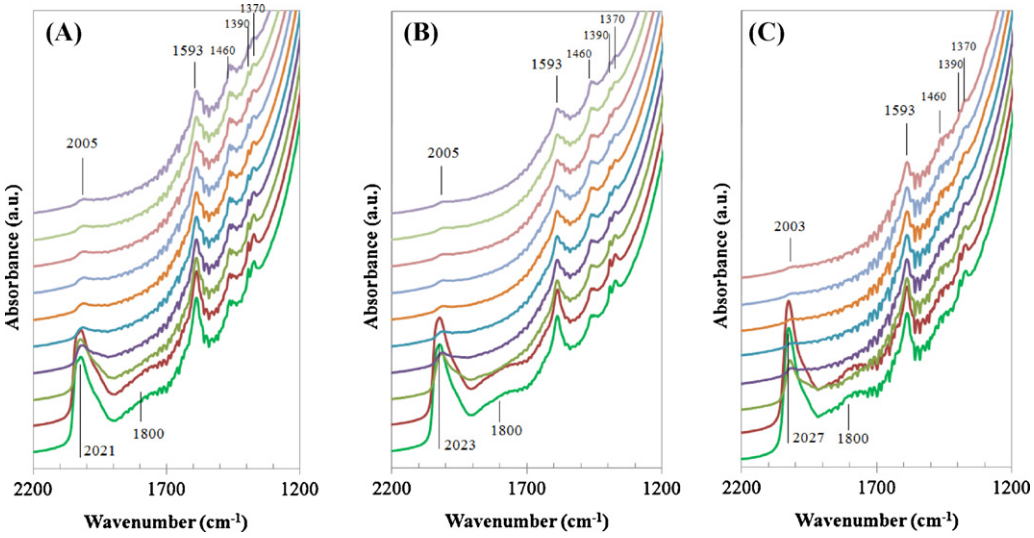

Fig. 6. DRIFT spectra for (A) Rh (1%)/γ-Al_2O_3, (B) Rh (2%)/γ-Al_2O_3, (C) Rh (5%)/γ-Al_2O_3 catalysts after the flow composed of H_2 (8 ml/min) + CO_2 (2 ml/min) + He (10 ml/min) is switched to H_2 (8 ml/min) + He (10 ml/min) at 200 °C. From bottom to top: before gas change, after 1, 5, 10, 15, 20, 25, 30, 35 and 40 min.

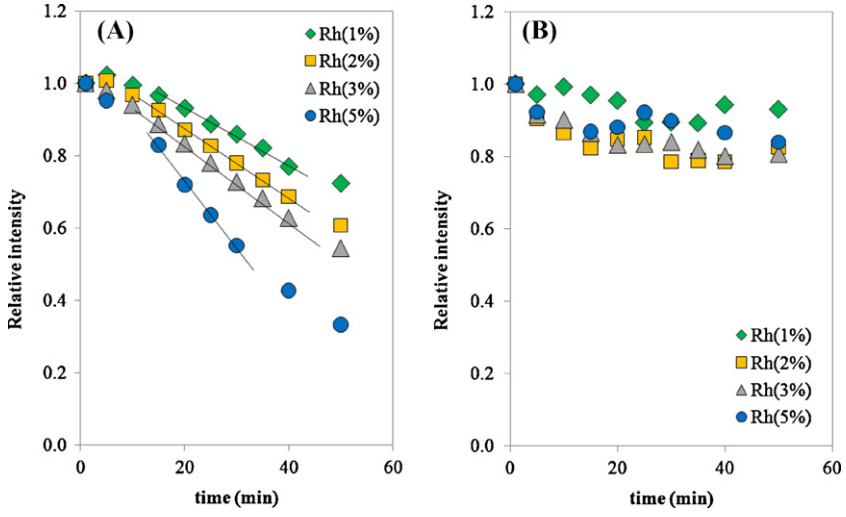

Fig. 7. DRIFTS normalized band intensity versus time after changing the gas feed from H_2 (8 ml/min) + CO_2 (2 ml/min) + He (10 ml/min) to H_2 (8 ml/min) + He (10 ml/min) at 150 °C. (A) Rh-CO band at 2050–2000 cm^{-1}. (B) Formate band at 1590 cm^{-1}. Lines are shown to indicate the region where rates were calculated.

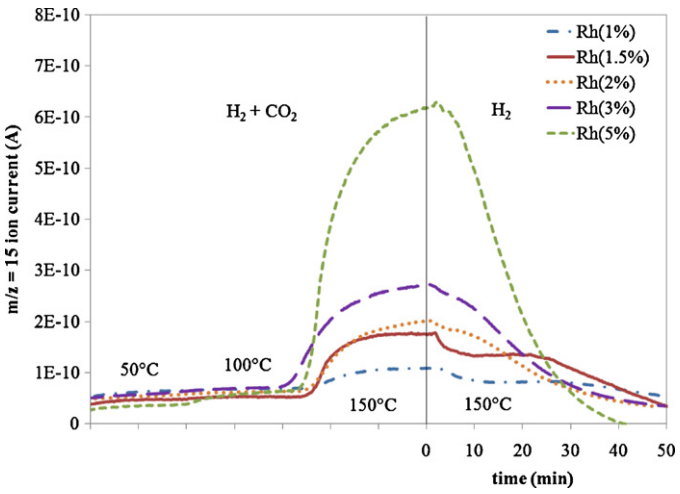

Fig. 8. Mass spectrometer analysis for Rh/γ-Al_2O_3 catalysts with different Rh content. Evolution of methane (m/z = 15) during heating in reactive mixture (H_2 (8 ml/min) + CO_2 (2 ml/min) + He (10 ml/min)) and subsequent transient in H_2 (8 ml/min) + He (10 ml/min) mixture at 150 °C.

disappearance is slower than in the case of purging in pure He. After 60 min under a flow containing hydrogen the peak is still intense, nevertheless it has shifted to lower wavenumbers, from 2032 to 2023 cm^{-1}. One can also observe the apparition of a peak at 1910 cm^{-1}, which has been assigned to $Rh_2(CO)_3$. The peaks due to surface formates (1590, 1390 and 1370 cm^{-1}) show a decrease in their intensities unlike the experiment performed with pure He. However, the band attributed to carbonates (1460 cm^{-1}) maintains its intensity.

In Fig. 10 it is shown the curves obtained by MS for methane (m/z = 15) and carbon dioxide (m/z = 44), in the same experiments described above. In panel A, we compare the evolution of methane detected at the exit of the DRIFTS cell when the catalyst (Rh(5%)/γ-Al_2O_3) is treated with He or H_2 + He after H_2 + CO_2 reaction. A difference in the dynamic behavior of the signals is observed. When the catalyst is treated with He, methane concentration decays faster than when the catalyst is exposed to H_2 + He flow, showing that in the latter case methane continues to be produced, whereas in the case of He flow no methane is produced. As a reference we plotted the behavior of the decrease in CO_2 signal (panel B), which is the same no matter one changes to He or H_2 + He flows.

4. Discussion

4.1. Activity of Rh/γ-Al_2O_3 catalysts toward CO_2 methanation

The rate of CH_4 formation of the Rh/γ-Al_2O_3 catalysts was found to be dependent on the dispersion of the active metal, in the range of dispersion studied (7–30%, or particle sizes from 3.6 to 15.4 nm). The turnover frequency (TOF) of methane formation decreases as dispersion increases in the low temperature range (135–165 °C, Fig. 1a), whereas for higher temperatures (185–200 °C) the TOF is independent of dispersion (Fig. 1b). In other words, the intrinsic rate of reaction is found to be independent of the size of Rh particles at high temperatures and slightly dependent when temperature is lower.

Literature data are scarce concerning the dependence of activity on the size of metallic particles for CO_2 methanation on noble metals. A recent study [18] using Ru/TiO_2 catalysts at 160 °C have shown that smaller Ru particles are the most active ones, with catalysts having a mean particle size of 2.5 nm being 15 times more active than those with Ru particles of 9.5 nm. Other authors have studied the CO_2 methanation as a part of selective methanation of CO [19], and have found that, for Ru/Al_2O_3 catalysts, the TOF of CO_2 consumption at 330 °C increases by a factor of 20 when particle size increases from 1.3 to 2.2 nm, but it is essentially constant from 2.2 to 13.6 nm. When Rh/Al_2O_3 was studied [19], TOF of CO_2 conversion decreases by a factor of 2.3 when particle size is decreased from 1.4 to 5.1 nm. It has to be considered that in these cases CO was also present in the gas phase and that part of CO_2 could be reacting in the reverse water gas shift reaction. Nevertheless, it is important to stress the marked effect of the type of metal, support and operating conditions on the main features of CO_2 methanation.

CO hydrogenation reaction has been studied much more extensively than CO_2 methanation. For that reaction, the trends observed in TOF versus particle size are in major part indicating that larger particles are the most active [45,46].

The first step in CO_2 hydrogenation is the adsorption and dissociation of CO_2 to CO(ads) and O(ads) while CO hydrogenation requires the direct adsorption of CO on the surface. Since afterwards both reactions require the dissociation of a C—O bond, it could be expected that the structural requirements and hence the trends of TOF versus particle size observed for CO_2 hydrogenation could be similar for CO hydrogenation. Our results show that this is not the case, which could suggest there are differences in the reaction pathway between these reactions.

The XPS results related to the distribution of Rh particles on γ-Al_2O_3 support give important insights. According to the results presented in Fig. 3, the XPS intensity ratio I_{Rh}/I_{Al} are larger than those predicted by the Kerkhof model assuming that the Rh atoms are dispersed as a monolayer on the surface of the support, that is, with maximum dispersion. Nevertheless, Rh is more probably forming small particles on alumina surface. When the content of Rh increases, the crystallites of Rh would grow, developing their lateral faces. If we assume that the metal particles are located on the external parts of the γ-Al_2O_3 particles, the XPS I_{Rh}/I_{Al} atomic ratio would be larger than assuming a homogeneous distribution of Rh on the surface of the support [47,48]. Table 1 shows that the size of the Rh mean particle increases with the Rh content, which is coherent with XPS measurements.

If we consider the variation of TOF with metal particle size at low temperature, it could be speculated that some particular sites, depending of the structure of the nanoparticles of Rh particles (lateral faces), are the most active in the CO_2 reaction. As the larger particles have a larger proportion of these lateral faces, their activity could be higher. On the contrary, small particles have a less important proportion of lateral faces and hence they would be less reactive. At temperatures between 185 and 200 °C, the TOF of methane formation was found to do not depend on particle size; at least in the studied interval of dispersions. This could indicate the different reactivity of Rh surfaces depending on temperature.

Regarding the activation energies found in this study, they vary between 14.5 and 22.7 kcal/mol and agree well with the values reported previously for Rh/Al_2O_3 in different intervals of temperature (16.2 kcal/mol between 135 and 200 °C [13], 17 kcal/mol between 160 and 240 °C [49] and 20.3 kcal/mol between 200 and 350 °C [50]). The activation energies obtained in this work (between 135 and 200 °C) tend to decrease with particle size (Table 2), which could be explained by the same reasons exposed above. Larger particles as those of Rh(3%)/γ-Al_2O_3 or Rh(5%)/γ-Al_2O_3 catalysts (15 nm particle size) show the lower activation energy (14.5 kcal/mol) and would have a bigger proportion of lateral faces compared with for instance Rh(1%)/γ-Al_2O_3 (22.7 kcal/mol, 3.6 nm). These lateral faces would favor the rate-limiting step hence decreasing the overall activation energy of the reaction.

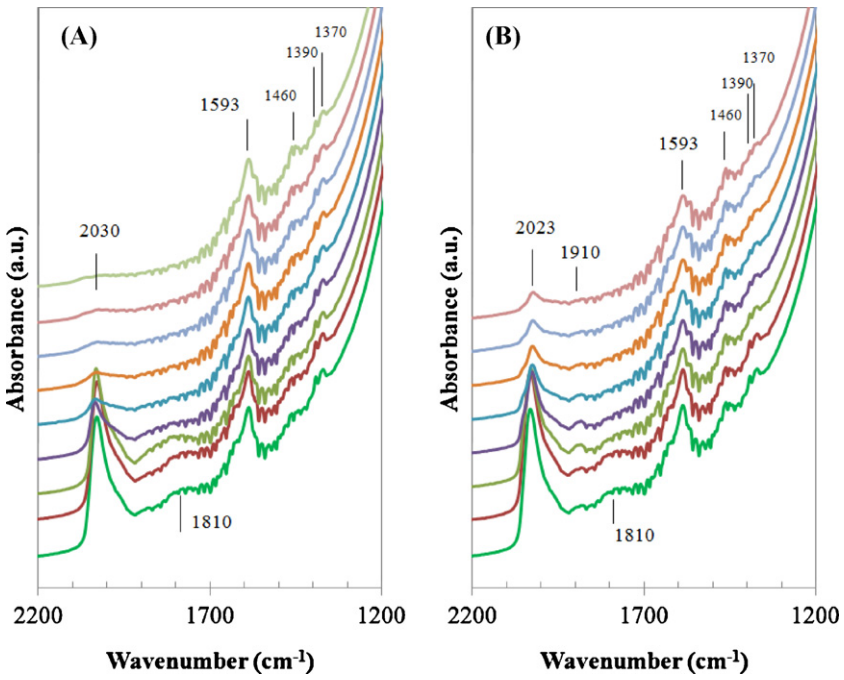

Fig. 9. Evolution of DRIFT spectra upon a change from CO_2 (2 ml/min) + H_2 (8 ml/min) + He (10 ml/min) stream to (A) He (18 ml/min) flow and (B) H_2 (8 ml/min) + He (10 ml/min) flow. Catalyst: Rh(5%)/γ-Al_2O_3. T = 150 °C. From bottom to top: H_2 + CO_2 + He before gas change, 1 min in He (or H_2 + He), 10, 20, 30, 40, 50 and 60 min.

4.2. Chemical state of Rh on γ-Al_2O_3 support

The binding energy of $Rh3d_{5/2}$ for calcined catalysts (309.7–309.8 eV, Table 3) corresponds to values assigned to irreducible Rh^{4+} species or Rh^{3+} in "super-stoichiometric" Rh_2O_3 with O/Rh higher than 1.5 [33]. Comparing the XPS spectra obtained for catalysts calcined with those obtained after reduction (Fig. 2), one can observe that the peak at 309.8 eV disappears and a new peak at 308.8 eV characteristic of Rh^{3+} species appears. The complete disappearance of the 309.8 eV peak after reduction at low temperature (350 °C) suggests that irreducible Rh is not present in these samples.

According to the results show in Table 3, the proportion of reduced Rh after reduction in H_2 or reaction is higher in the case of catalysts with high Rh content. It is known that γ-Al_2O_3 can interact with Rh metal supported on its surface, avoiding the reduction of metal particles [51]. This interaction is stronger when particles are smaller, which is in agreement with our results: Rh(1%)/γ-Al_2O_3 shows only a third of its superficial Rh in a reduced form whereas Rh(5%)/γ-Al_2O_3 has 69% of its superficial Rh reduced.

Nevertheless, the active state of Rh during the reaction is very likely to be Rh^0. As observed by in situ DRIFTS experiments, only Rh^0-$(CO)_z$ (z = 0.5, 1, 1.5) are detected. CO adsorbed on Rh^+, Rh^{2+} or Rh^{3+}, which would appear in the 2090–2135 cm^{-1} region [42], were not detected in any experiment. Nevertheless, Rh^{3+} species are detected by XPS. The absence of CO adsorbed on oxidized Rh sites could be due to: (a) that effectively CO is not adsorbed appreciably in oxidized Rh atoms in our experimental conditions; (b) that surface Rh is fully reduced during the reaction, and the oxidized Rh detected by XPS would come from oxidized Rh atoms located in the internal layers of the particles or (c) reduced Rh is oxidized during transport to XPS analysis chamber.

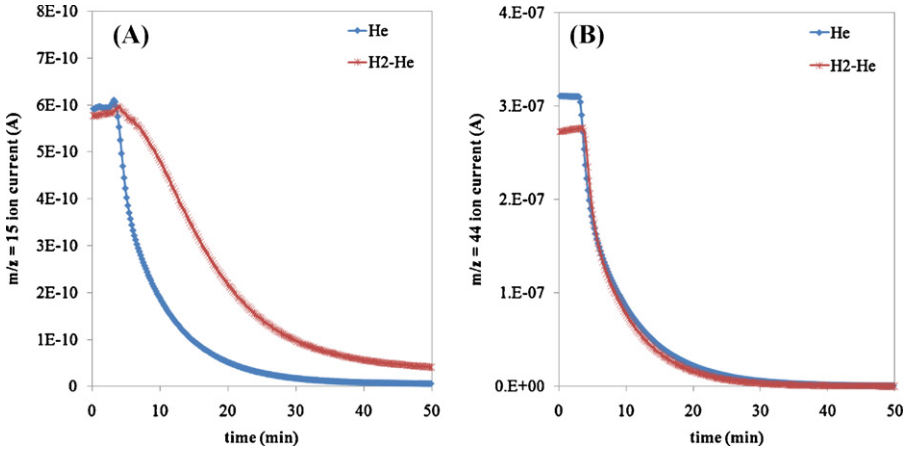

Fig. 10. Mass spectrometer responses for (A) m/z = 15 (CH_4) and (B) m/z = 44 (CO_2) resulting from the analysis of the gaseous products upon changing from CO_2 + H_2 + He feed to H_2 + He feed at 150 °C for Rh(5%)/γ-Al_2O_3.

4.3. CO_2 dissociation and related surface species

According to the results obtained in Fig. 4 for Rh/γ-Al_2O_3 catalysts during $H_2 + CO_2$ reaction, the apparition of Rh-CO band is detected at 50 °C over all the catalysts, which confirms the rapid hydrogen-aided dissociation of CO_2 on these catalysts. Similar results with the same catalysts have been showed in previous works using a pulse reactor [16,17].

The frequency at which Rh-CO peak is detected by DRIFTS is in the range 2036–2052 cm^{-1} and varies with Rh dispersion (i.e. particle size). Catalysts with low Rh dispersion (e.g. Rh(5%)/γ-Al_2O_3) have a higher frequency of adsorption comparing with catalysts with higher Rh dispersion (Rh(1%)/γ-Al_2O_3). The same phenomenon was observed in the case of CO hydrogenation on similar catalysts [52], which was explained in terms of increased electronic density in smaller metal particles due to support interaction effects, which could weaken the C—O bond and hence lead to a decrease in the frequency observed for adsorbed CO. In spite that this effect could be highly localized [36], the variation of CO adsorption frequency with particle size seems to be verified in the present study.

The frequency of the Rh-CO band is shifted to lower wavenumbers when the temperature is increased under $H_2 + CO_2$ flow (Fig. 4). It is also observed that the area of linear CO peak increases with temperature, implying an augmentation in CO coverage. The fact that coverage increases with temperature in the case of dissociative CO_2 adsorption has been already reported by Fisher and Bell over Rh/SiO_2 catalysts [23]. The fact that despite the increasing coverage the wavenumber of Rh-CO band decreases has been explained by the formation of Rh carbonyl hydride [13,23]. In Fig. 4C, the spectrum for Rh(5%)/γ-Al_2O_3 at 50 °C shows clearly two peaks in the CO frequency region, at 2052 and 2027 cm^{-1}. The peak appearing at higher frequency can be assigned to Rh-CO species, whereas the peak appearing at 2027 cm^{-1} could be ascribed to the carbonyl hydride species. Indeed, the 2027 cm^{-1} peak grows steadily with temperature whereas the peak at higher frequency disappears at 100 °C which could be due to the progressive transformation of Rh-CO species to Rh carbonyl hydride. The increased availability of H species at higher temperatures due to an enhanced rate of H_2 dissociation could be the responsible for this phenomenon. The same behavior can be observed for the other catalysts (Fig. 4A and B). The Rh-CO band presents a shoulder at lower frequencies, more clearly seen when the temperature is 50 °C. That can be ascribed to the incipient formation of carbonyl hydrides on these samples. These results show that when Rh content increases (Rh(5%)/γ-Al_2O_3), Fig. 4C, the peak ascribed to the carbonyl hydride species at 2027 cm^{-1} is observed already at low temperature (50 °C), and is larger comparing with catalysts with smaller particles. The easiness of Rh-carbonyl hydride formation over catalysts with larger particles, and hence with larger proportion of lateral faces, could be related to the higher activity of these catalysts.

4.4. The reactivity of adsorbed species

It has been proposed that the rate determining step of CO_2 methanation is the dissociation of CO_2 to CO(ads) species [7]. According to this results, it is observed that CO(ads) formation from CO_2 dissociation occurs readily at 50 °C, even when no methane is formed. This suggests that CO_2 dissociation is rapid enough and it is not controlling the overall rate of reaction.

Regarding the reactivity of the CO bands in hydrogen, it has been observed that bridged-bonded CO bands (1805 cm^{-1}) readily disappear in the transient experiments at both 150 and 200 °C, showing that they are more reactive than linear CO (Figs. 5 and 6).

The evolution of CO and formate bands in function of time (Fig. 7) is very indicative. The rate of formate consumption is much slower than the rate of consumption of Rh-CO species. These results confirm previous reports which proposed that formates are principally spectators in the reaction [24].

Comparing the rate at which Rh-CO band vanishes in transient experiments at 150 and 200 °C, one can calculate the apparent activation energy of this process. The results show (Table 4) that the activation energy of CO(ads) dissociation lie between 23 and 16 kcal/mol and compare well with the apparent activation energy of the whole reaction, which strongly suggests that C—O bond breaking is a key step in the reaction, which is in agreement with results presented previously [23].

Results show that at low temperature the CO is adsorbed only on metallic Rh, that the rate determining step of the reaction is the breaking of the C—O bond, and that the activation energy decreases and the TOF increases for the higher size particles, namely when the fraction of lateral faces increases. These results seem to suggest that the lateral faces of the Rh particles could play an important role in the reaction mechanism and more precisely in promoting the formation of Rh carbonyl hydride. The hydrogen atoms associated to CO could then help to dissociate C—O bond which increases the reaction rate. This effect could be more marked at low temperature since it was observed that particle size influence on turnover frequencies is more pronounced at low temperatures.

As seen in Fig. 9, after switching from reactive mixture ($H_2 + CO_2$) to pure He, CO band decreases faster comparing when changing to H_2 + He. This could be related to the different strength of CO adsorption on Rh. In the case of the presence of H_2 in the gas phase, the H atom of Rh carbonyl hydride enhances the strength of Rh—C bond while decreasing the strength of C—O bond [13]. This increases the rate of dissociation of CO species. When H_2 is absent, carbonyl hydrides disappear rapidly and CO is bonded to Rh as Rh-CO species instead of Rh carbonyl hydride form. This facilitates the desorption of CO(ads), without being hydrogenated. This can be observed by analyzing the position of the band related to adsorbed CO obtained for the two experiments. In both cases (reaction conditions at 150 °C) the initial position of CO band is nearly the same (2030 cm^{-1}). When $H_2 + CO_2$ mixture is switched to He, the CO band decreases in intensity while its frequency is unchanged, which could be due to the compensating effect of, on the one hand, the disappearance of carbonyl hydrides and on the other the decrease in CO coverage; both phenomena having an opposite effect on the measured frequency of Rh-CO peak. When H_2 is present, the shift to lower wavenumbers is clearly seen, which implies that carbonyl hydrides are present during hydrogenation, even when coverage has decreased significantly.

The desorption of CO from Rh/γ-Al_2O_3 catalysts generally occurs at temperatures between 150 and 250 °C [53,54]. The rapid desorption observed at 150 °C in presence of He could be promoted by the interaction of γ-Al_2O_3 hydroxyls with adsorbed CO, which is known to enhance the rate of desorption [54].

The fact that in the case of the transient experiment in presence of H_2 methane is produced is confirmed by MS analysis of the effluent of the DRIFTS cell. When the carbonyls where flushed with He no CH_4 was detected.

Regarding formate species, their stability in the case of He flushing at 150 °C (Fig. 9) is higher than for Rh-CO species. Formate bands at 1370–1390 cm^{-1} and 1593 cm^{-1} are stable throughout the experiment unlike the experiment in presence of H_2 where the intensity of formate bands decrease although not completely, indicating that they could participate in the reaction pathway but, would have a minor influence.

The mechanism sequence after the H helped dissociation of CO could led to CH species which are rapidly further hydrogenated to give CH_4. The rapidity of these steps could be confirmed by the absence of CH*x* species in the DRIFT spectra.

4.5. Methanation at high and low temperature

Comparing CO_2 methanation performed at high and low temperature, our results show that activation energies are similar, in the range 15–22 kcal/mol. Nevertheless, the decrease in activation energy with increasing particle size has not been reported previously, even at higher temperatures.

An important aspect to be underlined is the selectivity of the reaction. Our results show that CO_2 methanation is highly favored at low temperatures. In all experiments performed in this work, the selectivity was 100%. At temperatures higher than 200 °C, CO formation is favored by the reverse water gas shift reaction. When the reaction is carried out at high temperatures, the selectivity is significantly lower than 100% [50].

On the other hand, our results are in line with previous works obtained for the methanation of CO_2 at temperatures comparable with those employed in the present study (130–200 °C) [13,41]. They concluded that CO_2 dissociation is favored by the presence of H_2 and that formates species are located on the support and do not contribute to the reaction mechanism. Nevertheless, our results differ with previous studies which claims that the CO formation occurs through the reverse water-gas shift reaction in which CO_2 reacts with H(ads) to give formates and eventually CO adsorbed species [10]. In our case (temperature <200 °C), reverse water gas shift is not occurring (CO is absent in gas phase), which could discard this mechanism as the path for CO(ads) formation.

CO_2 methanation has been studied at 190 °C over Ru/Al_2O_3 and Ru/zeolite catalysts. It has been proposed that HCO(ads) species are the main reaction intermediate, although these species were observed only on Ru/Al_2O_3 catalyst [24]. CO_2 dissociation leads to the formation of adsorbed CO which is thought to be associated with hydrogen to form Rh carbonyl hydride. If it is assumed that the H atoms help to dissociate C—O as was recently proposed [55], it could be suggested that catalysts which could facilitate hydrogen dissociation and mobility at temperatures low enough, will help to increase the catalytic performances. In this process the control of the size of the particles is primordial.

In this work, the experimental parameters which could allow improving performances in CO_2 methanation are given. The probable rate-determining step of this reaction is discussed. The fact that at low temperature the selectivity in the formation of methane is 100%, strongly suggests that this process could be an important alternative to use CO_2 to obtain high value-added products which could be used in chemical and petrochemical industry.

5. Conclusions

CO_2 methanation at low temperatures was studied over Rh/γ-Al_2O_3 catalysts. Catalysts with varying Rh content gave rise to different Rh particle sizes (between 3.6 and 15.4 nm). Selectivity to methane was 100% over the entire range of temperature and Rh loadings studied. The turnover frequency for CH_4 formation was found to be dependent on Rh particle size. Larger Rh particles are up to four times more active than smaller particles at low temperature (135–150 °C), whereas at higher temperatures (200 °C) the turnover frequencies are similar for all particle sizes. Apparent activation energies were found to be in the range 14.5–22.7 kcal/mol, and to depend on Rh particle size. Catalysts with smaller particles have the higher activation energies, which can be explained in terms of the structure sensitivity of the reaction.

Results of *operando*-DRIFTS experiments show that CO_2 adsorption and dissociation occurs readily over the catalysts when H_2 is present, resulting in the formation of linear Rh-CO species, bridged $Rh_2(CO)$ and $Rh_2(CO)_3$ species, the last two are more abundant in catalysts with larger particles. Nevertheless, linearly adsorbed CO accounts for the majority of the species formed. From the analysis of the variations in the position of Rh-CO band as a function of CO coverage and temperature, it is suggested that linearly adsorbed CO is associated with H to form Rh carbonyl hydride.

Evidence is provided that CO(ads) species are the precursors of methane. The disappearance of these species in transient experiments under H_2 as observed by DRIFTS correlates well with the formation of methane. Moreover, comparing the activation energy obtained for the overall reaction with the activation energy obtained for the reaction of CO(ads) species with hydrogen, it is suggested that H-aided C—O bond breaking is a key step in CO_2 methanation on these catalysts. Formates are proposed to be spectator species and do not contribute significantly to methane formation.

Acknowledgments

The authors gratefully acknowledge the “Direction Générale des Technologies, de la Recherche et de l’Energie (DGTRE)” of the “Région Wallonne” (Belgium) and the“Fonds National de la Recherche Scientifique (FNRS)” of Belgium, for their financial support. The involvement of IMCN-MOST in the «INANOMAT» IUAP network sustained by the « Service public fédéral de programmation politique scientifique» (Belgium) is acknowledged. AK thanks the “BecasChile” program of CONICYT (Chile) for his PhD research grant.

References

[1] G. Centi, S. Perathoner, Catal. Today 148 (2009) 191–205.
[2] M. Aresta, A. Dibenedetto, Dalton Trans. (2007) 2975–2992.
[3] E.W. McFarland, J.N. Park, J. Catal. 266 (2009) 92–97.
[4] H. Metiu, S. Sharma, Z.P. Hu, P. Zhang, E.W. McFarland, J. Catal. 278 (2011) 297–309.
[5] G.D. Weatherbee, C.H. Bartholomew, J. Catal. 87 (1984) 352–362.
[6] G.D. Weatherbee, C.H. Bartholomew, J. Catal. 77 (1982) 460–472.
[7] M. Marwood, R. Doepper, M. Prairie, A. Renken, Chem. Eng. Sci. 49 (1994) 4801–4809.
[8] F. Solymosi, A. Erdohelyi, M. Kocsis, J. Chem. Soc. Faraday Trans. 1 (77) (1981) 1003–1012.
[9] S. Scire, C. Crisafulli, R. Maggiore, S. Minico, S. Galvagno, Catal. Lett. 51 (1998) 41–45.
[10] D.I. Kondarides, P. Panagiotopoulou, X.E. Verykios, J. Phys. Chem. C 115 (2011) 1220–1230.
[11] R.J. Behm, S. Eckle, Y. Denkwitz, J. Catal. 269 (2010) 255–268.
[12] A. Erdohelyi, M. Pasztor, F. Solymosi, J. Catal. 98 (1986) 166–177.
[13] F. Solymosi, A. Erdohelyi, T. Bansagi, J. Catal. 68 (1981) 371–382.
[14] T. Iizuka, Y. Tanaka, K. Tanabe, J. Mol. Catal. 17 (1982) 381–389.
[15] Z.L. Zhang, A. Kladi, X.E. Verykios, J. Catal. 148 (1994) 737–747.
[16] M. Jacquemin, A. Beuls, P. Ruiz, Catal. Today 157 (2010) 462–466.
[17] A. Beuls, C. Swalus, M. Jacquemin, G. Heyen, A. Karelovic, P. Ruiz, Appl. Catal. B 113–114 (2012) 2–10.
[18] T. Abe, M. Tanizawa, K. Watanabe, A. Taguchi, Energy Environ. Sci. 2 (2009) 315–321.
[19] P. Panagiotopoulou, D.I. Kondarides, X.E. Verykios, Ind. Eng. Chem. Res. 50 (2010) 523–530.
[20] M. Kusmierz, Catal. Today 137 (2008) 429–432.
[21] W. Rarog-Pilecka, Z. Kowalczyk, K. Stolecki, E. Miskiewicz, E. Wilczkowska, Z. Karpiniski, Appl. Catal. A 342 (2008) 35–39.
[22] P. Panagiotopoulou, D.I. Kondarides, X.E. Verykios, Appl. Catal. B 88 (2009) 470–478.
[23] I.A. Fisher, A.T. Bell, J. Catal. 162 (1996) 54–65.
[24] S. Eckle, H.-G. Anfang, R.J.r. Behm, J. Phys. Chem. C 115 (2010) 1361–1367.
[25] J.N. Park, H.Y. Kim, H.M. Lee, J. Phys. Chem. C 114 (2010) 7128–7131.
[26] C. Force, A. Ruiz Paniego, J.M. Guil, J.M. Gatica, C. López-Cartes, S. Bernal, J. Sanz, Langmuir 17 (2001) 2720–2726.
[27] F.P.J.M. Kerkhof, J.A. Moulijn, J. Phys. Chem. 83 (1979) 1612–1619.
[28] J.H. Scofield, J. Electron Spectrosc. Relat. Phenom. 8 (1976) 129–137.
[29] S. Tougaard, QUASES-IMFP-TPP2M software, Quases-Tougaard Inc., 2002.
[30] S. Tanuma, C.J. Powell, D.R. Penn, Surf. Interface Anal. 21 (1994) 165–176.
[31] M.A. Vannice, Kinetics of Catalytic Reactions, Springer, New York, 2005.
[32] M. Kawai, M. Uda, M. Ichikawa, J. Phys. Chem. 89 (1985) 1654–1656.
[33] Z. WengSieh, R. Gronsky, A.T. Bell, J. Catal. 170 (1997) 62–74.
[34] J.S. Brinen, A. Melera, J. Phys. Chem. 76 (1972) 2525–2526.
[35] H.Y. Luo, H.W. Zhou, L.W. Lin, D.B. Liang, C. Li, D. Fu, Q. Xin, J. Catal. 145 (1994) 232–234.

[36] J.C. Lavalley, J. Saussey, J. Lamotte, R. Breault, J.P. Hindermann, A. Kiennemann, J. Phys. Chem. 94 (1990) 5941–5947.
[37] C. Yang, C.W. Garl, J. Phys. Chem. 61 (1957) 1504–1512.
[38] B.A. Riguetto, S. Damyanova, G. Gouliev, C.M.P. Marques, L. Petrov, J.M.C. Bueno, J. Phys. Chem. 108 (2004) 5349–5358.
[39] V.S. Kamble, V.P. Londhe, N.M. Gupta, K.R. Thampi, M. Grätzel, J. Catal. 158 (1996) 427–438.
[40] H. Wijnja, C.P. Schulthess, Spectrochim. Acta, Part A 55 (1999) 861–872.
[41] F. Solymosi, A. Erdohelyi, T. Bansagi, J. Chem. Soc. Faraday Trans. 1 (77) (1981) 2645–2657.
[42] S.S.C. Chuang, R.W. Stevens, R. Khatri, Top. Catal. 32 (2005) 225–232.
[43] W.M.H. Sachtler, M. Ichikawa, J. Phys. Chem. 90 (1986) 4752–4758.
[44] P.B. Rasband, W.C. Hecker, J. Catal. 139 (1993) 551–560.
[45] M. Che, C.O. Bennett, H.P.D.D. Eley, B.W. Paul (Eds.), Advances in Catalysis, Academic Press, 1989, pp. 55–172.
[46] G.L. Bezemer, J.H. Bitter, H.P.C.E. Kuipers, H. Oosterbeek, J.E. Holewijn, X. Xu, F. Kapteijn, A.J. van Dillen, K.P. de Jong, J. Am. Chem. Soc. 128 (2006) 3956–3964.
[47] V. Leon, Surf. Sci. 339 (1995) L931–L934.
[48] A. Cimino, D. Gazzoli, M. Valigi, J. Electron Spectrosc. Relat. Phenom. 104 (1999) 1–29.
[49] T. Iizuka, Y. Tanaka, K. Tanabe, J. Catal. 76 (1982) 1–8.
[50] P. Panagiotopoulou, D.I. Kondarides, X.E. Verykios, Appl. Catal. A 344 (2008) 45–54.
[51] C.P. Hwang, C.T. Yeh, Q.M. Zhu, Catal. Today 51 (1999) 93–101.
[52] Y. Mori, T. Mori, A. Miyamoto, N. Takahashi, T. Hattori, Y. Murakami, J. Phys. Chem. 93 (1989) 2039–2043.
[53] A. Erdohelyi, F. Solymosi, J. Catal. 84 (1983) 446–460.
[54] D.A. Bulushev, G.F. Froment, J. Mol. Catal. A: Chem. 139 (1999) 63–72.
[55] I. Chorkendorff, M.P. Andersson, E. Abild-Pedersen, I.N. Remediakis, T. Bligaard, G. Jones, J. Engbwk, O. Lytken, S. Horch, J.H. Nielsen, J. Sehested, J.R. Rostrup-Nielsen, J.K. Norskov, J. Catal. 255 (2008) 6–19.